PHILIPPINE ENGINEERING JOURNAL
PEJ 2023; Vol. 44, No. 1: 25-44

Received: 27 August 2022
Accepted: 04 March 2023

Air Change Rates and Aerosol Dispersion in a Room with Ceiling and Stand Fans Using Computational Fluid Dynamics

Ken Bryan A. Fernandez[1], Jeffrey E. Silva[2] and Edwin N. Quiros[1]
[1]Department of Mechanical Engineering, University of the Philippines Diliman, Quezon City, Philippines
[2]Energy Engineering Graduate Program, University of the Philippines Diliman, Quezon City, Philippines

Abstract - *Previous study demonstrated the effect of a single fan in terms of air change per hour (ACH) and air evacuation rate in a room to mitigate airborne diseases. With the goal of finding cheaper and short-term solutions to replace expensive and long-term dedicated ventilation systems, this study performed computational fluid dynamics simulations to determine the effect of adding another fan (ceiling or stand fan) on the ACH, particle dispersion, and maximum particle time. Ten cases, 2 push-pull and 8 stand fan and ceiling fan combinations, were investigated in a room with two openings: a door and a window. Two aerosol source locations were considered: 1) the occupant near the door as the infector 2) the occupant near the window as the infector. Results show that the push-pull configurations generated higher ACHs (46.33 and 51.60) that are approximately near the sum of the ACH of push-only and pull-only cases. In addition, the stand fan with ceiling fan cases may or may not increase the ACH depending on whether the induced flow is in the same direction with the flow generated by the initially installed fan. Nevertheless, the intake stand fan placed at the window boundary coupled with ceiling fan facing the downward direction generated the highest ACH of 55.92. On the other hand, the addition of a fan generally increased the velocities inside the room, increasing the particle deposition on the surfaces rather than being evacuated outdoors. The FDI-FWE of the M1 case generated the highest particle evacuation rate of 14.96%. Lastly, the maximum particle time can decrease because of two reasons: 1) particles are easily deposited on the surfaces due to higher velocities, 2) particles are easily evacuated after generation, while it can increase when the particles enter a stagnation or recirculation zone.*

Keywords: Air change rate, Indoor Air Quality, Stand and Ceiling Fans, Particle Dispersion, Computational Fluid Dynamics, COVID-19

I. INTRODUCTION

Typical air-conditioning systems in the Philippines are designed for energy efficiency, where the conditioned air just circulates inside the room, and the ventilation or the introduction of fresh air from outdoors is solely reliant on the frequent opening of doors due to people entering and exiting the room and other possible paths such as building cracks and holes. With the COVID-19 virus being spread through airborne routes [1], [2], such systems are unfavorable. Moreover, although having buildings with dedicated ventilation systems is the way forward, short-term solutions should be implemented.

To avoid the accumulation of aerosols generated by an infected person, dilution and exhaustion of indoor air is necessary through air exchange with outdoor air (assumed clean) [3]. This exchange can be quantified by air flow rate at the openings or by how many times the indoor air is replaced by the fresh outdoor air, typically on an hourly basis, called air change rate per hour (ACH) [4].

For rooms without dedicated ventilation systems, opening of windows and doors and the addition of fans to introduce fresh air from outdoors or exhaust stale (contaminated) air from indoors can increase the ACH. Another guiding principle that should be considered is the air flow patterns that determine the dispersion behavior of the aerosols generated by the infected person [5]. Questions such as whether the particles will be exhausted outdoors, deposited on surfaces, transferred to the healthy occupants, and accumulated for a longer period in stagnation and recirculation zones, should be addressed.

Although experimental studies provide realistic and substantial reports on the air change rate (and flow rate) and air flow patterns concerning airborne diseases [5]–[12], such methodology is heavily dependent on the number and quality of velocity measuring devices and imaging equipment. Alternatively, using digital computers, the discipline of computational fluid dynamics (CFD) generates quantitative forecasts of fluid-flow phenomena based on the conservation equations (conservation of mass, momentum, and energy) regulating fluid motion [13]. Through its validation with the previous field and wind tunnel experiments, the CFD method has been a cheaper alternative to predict the flow dynamics accurately.

Prior CFD studies were conducted to study the effect of the opening of doors and windows (extending to window geometry or wind catchers) in terms of ACH (or flow rate), particle dispersion behavior, and even CO2 distribution (alternative for particle dispersion). Abuhegazy et al.[14] showed that through opening of windows, the exit fraction of the particle generated by the occupants can be increased by around 38%. Lipinski et al. [15] compared two different wind catcher configurations that produced 2.5 to 3.3 ACH and low indoor CO2 levels. Abdo et al. [16] focused on the comparison of different window inlet design that can increase the volume flow rate by 2.55 – 8.44 %. On the other hand, He et al. [17] enhanced the ventilation efficiency of a room by adding a roof window. Aside from doors and windows, stand fans and ceiling fans have been proven to increase the room ACH and can potentially improve the consequent particle transport inside the indoor space. For example, the studies of Alotaibi et. al [5] and El-Fil et al. [10] optimized the settings of a ceiling fan coupled with a desk or chair mounted fan to produce better particle concentration distribution and energy savings. On the other hand, Li et al. [9] paired a currently installed AC system with a ceiling fan and produced more concentration distribution at higher fan speeds. Furthermore, Fernandez et al. [18] investigated the effect of adding a stand fan located at the window or door of an office room and showed that different fan placement locations can result in different ACH and then particle evacuation rate. They also discussed that higher ACH does not necessarily mean high particle evacuation rate.

With the goal of finding more strategies on how to mitigate the COVID-19 infections for face-to-face classes and office works in the Philippines, this study aimed to extend the previous works particularly the study of Fernandez et al. [18] by adding an additional fan that can be either a stand fan or a ceiling fan as these devices are commonly found in typical classrooms, offices, and households. We first added a ceiling fan to the previous 4 single fan cases. Unlike the previous studies, we allowed the ceiling fan to face either the downward or upward directions - making a total of 8 stand fan plus ceiling fan combinations. In addition, we also explored the push-pull configurations using stand fans that were placed at both boundaries (window and door). CFD simulations were done to compute for the ACH and the resulting aerosol transport (whether it will get evacuated from the room or deposited on the surfaces) of the 10 combinations and were

compared with the results of the previous single fan study. Lastly, the maximum particle time that determines the age of the oldest generated particle inside the room were analyzed to understand its relationship with the particle dispersion.

II. METHODOLOGY

2.1 Computational Domain

To compare the effects of an additional stand fan or ceiling fan, this study utilized the same room that was previously used in the research of Fernandez et al. [18]. Isothermal simulations were conducted for a single room in University of the Philippines Diliman with dimensions of 6731mm by 3429mm by 2690mm. A door and a window, measuring 889mm by 2083mm and 1170mm by 1470mm, respectively, were included as possible inlet/outlet of the flow field. Additionally, two occupants (one infected and one healthy) with their respective chairs, desks, and computers were modeled inside the room (Figure 1).

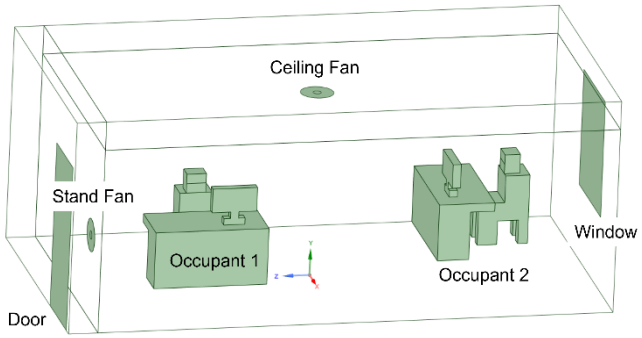

Figure 1. Room Lay-out with Occupants

2.2 Fan and Model Cases

The stand and ceiling fans were identically modeled with the following dimensions: 41mm outer diameter and 10mm inner diameter (hub diameter), and then through the use of the infinitely thin surface internal boundary condition based on the validation done by Krol et al. [19]. Moreover, fan pressure drop and tangential velocity of 16.711 Pa and 0.6 m/s, respectively, served as the inputs for the fan model to drive the flow based on the experiments and simulations done by Fernandez et al. [18] for a generic fan operated at maximum speed with the thin surface boundary placed 1 foot away from the center of either of the door, window, or ceiling. In their study, the input values of the fan were determined by making the CFD and experimental fan velocities are the same. Here, the stand fan is allowed to be used as exhaust or intake of the domain, while the ceiling fan is allowed to face the downward or upward directions. Therefore, the door (or window) stand fan can be as exhaust or intake and can be paired with either ceiling fan facing upward or downward directions - generating a total of 8 combinations of stand fan plus ceiling fan. In addition, two push-pull stand fan combinations were added: door fan as intake while the window as exhaust, and door fan as exhaust and window fan as intake. The summary of the 10 combinations is presented in (Figure 2).

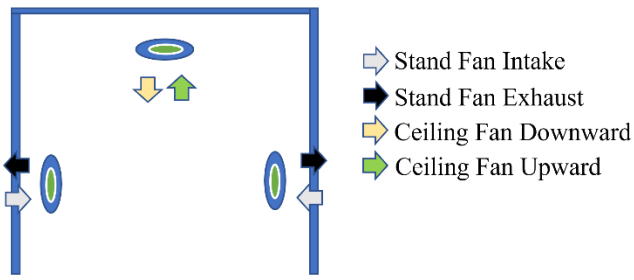

Combinations	
FDE-CU	Door Exhaust + Ceiling Upward
FDE-CD	Door Exhaust + Ceiling Downward
FDI-CU	Door Intake + Ceiling Upward
FDI-CD	Door Intake + Ceiling Downward
FWE-CU	Window Exhaust + Ceiling Upward
FWE-CD	Window Exhaust + Ceiling Downward
FWI-CU	Window Intake + Ceiling Upward
FWI-CD	Window Intake + Ceiling Downward
FDE-FWI	Door Exhaust + Window Intake
FDI-FWE	Door Intake + Window Exhaust

Figure 2. Stand Fan and Ceiling Fan Combinations

2.3 Numerical Scheme

ANSYS Fluent, which utilizes the finite volume method for incompressible continuity and RANS equations (Eq. (1) and Eq. (2), was used to perform three-dimensional CFD simulations. The exact solutions of the Navier-Stokes equations are very hard and in some cases, impossible to solve. Techniques were used to approximate the solutions, and one of the techniques, among others, is the Reynolds-averaged Navier-Stokes (RANS) model, wherein flow variables are decomposed into mean and fluctuating components. Although the mean part was resolved, the fluctuating component still appear in the RANS equation in the form of Reynolds stress. To solve the Reynolds stress term, there is a need to model it; such modeling is called the closure problem and is solved using different turbulence models.

$$\frac{\partial U_i}{\partial x_i} = 0 \tag{1}$$

$$\rho \frac{\partial U_i}{\partial t} + \rho U_j \frac{\partial U_i}{\partial x_j} = -\frac{\partial P}{\partial x_i} + \frac{\partial}{\partial x_j}\left(2\mu S_{ij} - \rho\overline{u_i' u_j'}\right) \tag{2}$$

where ρ denotes the fluid density, U_i and U_j represent the mean (time-averaged) fluid velocity components, P pertains to the pressure, x_i and x_j are the position vectors and S_{ij} is the mean rate of strain tensor. Take note that the term $\rho\overline{u_i' u_j'}$ represents the Reynolds stress.

In this study, the authors chose the k-ε realizable turbulence model mainly because it was the one used by the previous study (single fan case study of Fernandez et al. [18]) where we will compare our results. We want to eliminate new factors arising from using another turbulence model. In addition, the k-ε realizable turbulence model, which was proposed by Shih et al. [20], is a two-equations model with improved performance in flows exhibiting strong adverse pressure gradients and separation zones compared to the more popular standard k-ε model. Such flow conditions are characteristics of our study. Meanwhile, the drawback of this turbulence model is

that it produces non-physical turbulent viscosities typically found in situations with both stationary and rotating fluid zones such as rotating sliding meshes or multiple reference frames [21]. These types of situations were absent in our study. Furthermore, previous indoor airflow RANS simulations (also using the k-ε realizable turbulence model) with similar characteristics with the present study were conducted such as in the works of Alotaibi et al. [5], El-Fil et al. [10], and Habchi et al. [11] for the case of a room with ceiling and desk fans. Lastly, we followed the solver numerical schemes of Fernandez et al. [18] – pressure-based coupled scheme, least squares cell-based scheme for gradient, second order scheme for pressure transport, and second order upwind scheme for both the momentum and turbulence transport [22].

2.4 Mesh Independence and Time Independence Study

The current study used the hexahedral-dominant cut-cell method meshing technique. A trade-off between simulation time and accuracy of results was investigated by finding the optimal sizes of mesh and time-step. The authors studied four element sizes: 25 mm (~3,900,000 elements) for the finest mesh, 50 mm (~500,000 elements) for the fine mesh, 100 mm (~80,000 elements) for the medium-sized mesh, and 200 mm (~30,000 elements) for the coarse mesh. Initial steady-state simulations for all the 10 cases were done – making a total of 40 simulations. Presented in *Figure 3*a are the mass flow rates at the inlet (or outlet) boundary of 50mm, 100mm, and 200mm results in comparison with the 25mm. In the figure, the FDI-CU, FWI-CD, FDE-FWI cases were used as examples. With the criterion of less than 5% error with respect to the value of the 25mm, the succeeding simulations used the 100mm mesh size (*Figure 3*b) for each of the cases. Generally, the following are the final mesh parameters of the individual meshes used: average aspect ratio of 1.12, average skewness of 0.0018, and average orthogonal quality of 0.98.

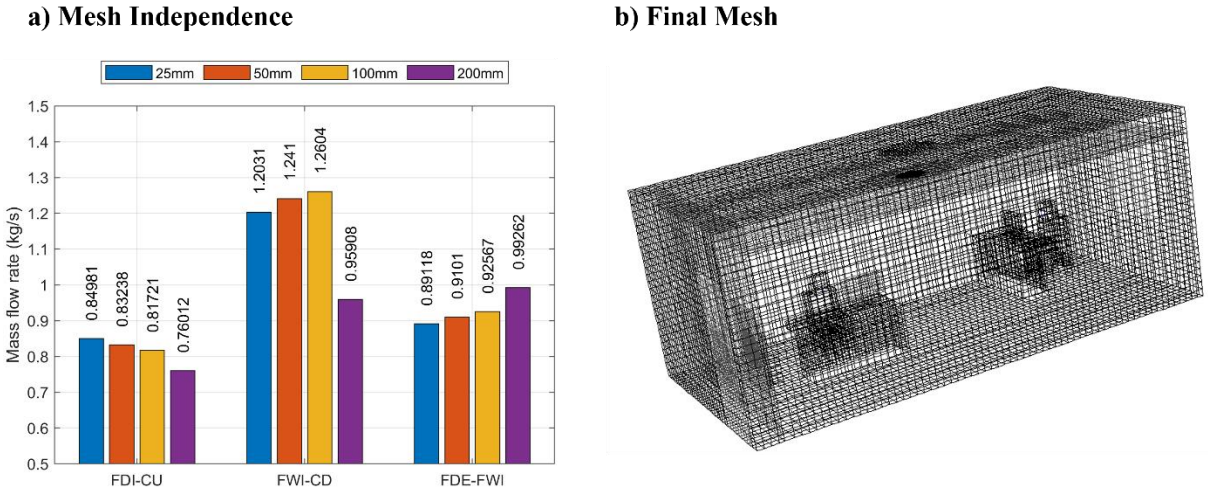

Figure 3: (a) Mesh Independence Mass Flowrate Comparison and (b) Final Mesh Size

After obtaining the mesh size, the time-step was determined by setting the size to 0.0002 seconds where the maximum courant number can be maintained to ≤ 1 [23]. The time-step size was then varied by multiples of 10: 0.002 and 0.02 seconds and were compared with the 0.0002 for the first 60 seconds of the flow time. This was repeated for each of the two-fan combinations. As an example, *Figure 4* shows the time-step comparison of the FDI-CD configuration. As

speculated in the previous study [18], higher time-step sizes generate high maximum Courant number but only for small regions of the domain, which does not affect the general behavior of the flow field. This is also the case for the other configurations; thus, a time-step of 0.02 seconds was adopted for the succeeding sections.

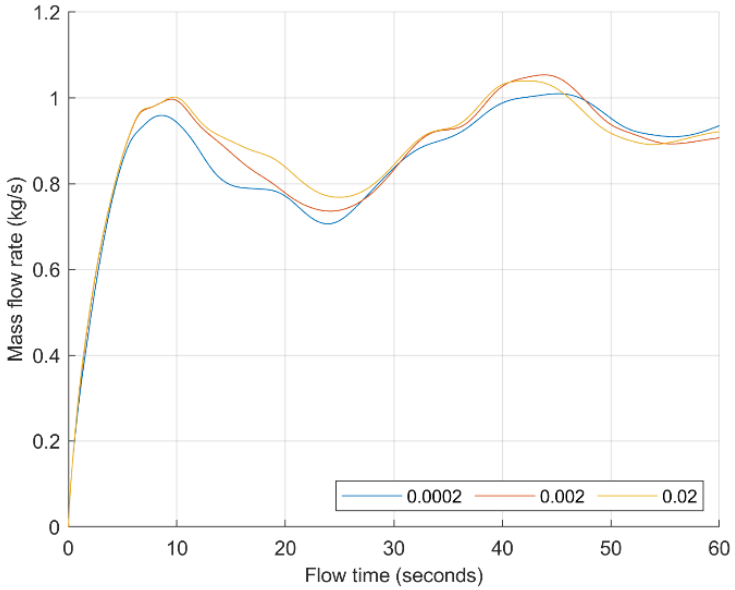

Figure 4. Time-step Independence – FDI-CD Configuration

2.5 Particle Generation and Trajectories

This study conducted two particle generation cases: M1, where the infected particles are generated by the occupant near the door and M2, where the infected particles are generated by the occupant near the window. To easily compare the particle dispersion of our current study with the results of the previous single fan cases of Fernandez et al. [18], and to eliminate possible additional effects of using other models, we also utilized the Lagrangian discrete phase model with the same settings to determine the particle trajectories. Also, this model has been widely used in previous indoor ventilation studies where particles are generated by human activities such as breathing, coughing, and sneezing [24]–[28]. The model (*Eq. (3)*) predicts the trajectories based on the external forces brought by the fluid phase. Here, the Saffman lift, virtual mass, pressure gradient forces, and other forces were also not considered, and the discrete phase was not assumed to affect the fluid phase. We adopted the default particle time-step size, and the number of particles generated were dependent on the number of faces on the infectors mouth. We also neglected the evaporation and growth rate of particles – setting a uniform aerosol size (water vapor) of 0.26 microns considering occupants with surgical masks [29]–[31]. The breathing with coughing event from Fernandez et al. [18] was utilized and the particles were injected starting from the 60 seconds flow time until the end of the simulation (240 seconds flow time). Lastly, the particle fates were summarized in *Table 1*.

$$\frac{du_p}{dt} = F_d(u - u_p) + \frac{g_x(\rho_p - \rho)}{\rho_p} + F_x \quad (3)$$

where u is the fluid phase velocity, u_p is the particle velocity, ρ is the fluid density, ρ_p is the particle density, F_d is the drag force, and F_x are the other forces [21].

Table 1. Particle Fate

Boundary	Particle Fate
Door	Escape
Window	Escape
Floor, ceiling, and walls	Trap
Occupants' worktables' surfaces	Trap
Infected Occupant's mouth	Escape
Healthy Occupant's mouth	Escape

2.6 Air Change Rate Computation

After determining the mass flow rates, the ACHs of the configurations were determined using the equation:

$$ACH = \frac{\dot{m}}{\rho V_{room}} \quad (4)$$

where $\dot{m}$ is the mass flow rate in either of the window or door, and V_{room} is the volume of the room.

III. RESULTS AND DISCUSSION

3.1 Air Change Rate

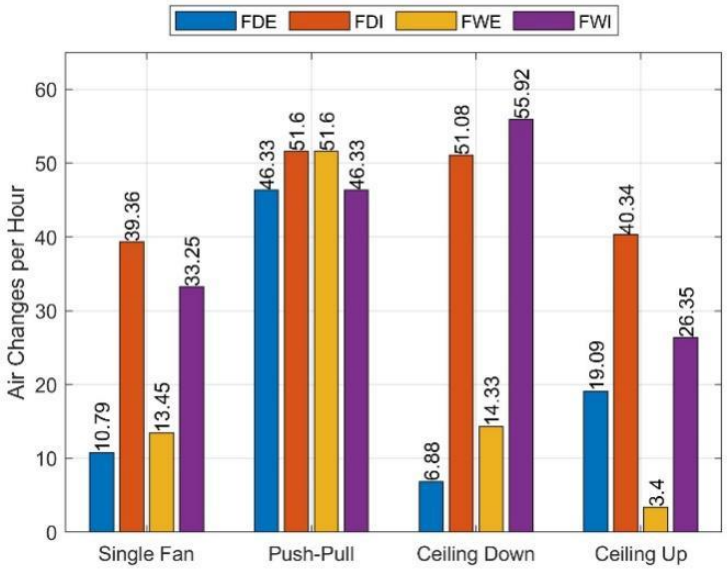

Figure 5. Air Change Rates of Single Fan and Dual Fan Configurations

Presented in *Figure 5* are the ACHs of the 10 double-fan new cases together with the single-fan cases from the previous research [13]. It should be noted that there are 4 cases for push-pull configuration in the figure since we also showed the FWE-FDI and FWI-FDE cases even though they have the same values as the FDI-FWE and FDE-FWI cases, respectively. Here, the mass flow rates for each case were taken by averaging starting from the 60 seconds flowtime where the mass flow rates are stable or oscillate at a certain value. These average mass flow rates were then used to compute for their individual ACH using *Eq. (4)* to compare the effect of an additional fan. For the push-pull configurations, it can be observed that installing an additional and complementing fan to the other side of the room to form a push-pull (e.g. from the previous single exhaust fan at the door location to a push-pull by an additional intake fan at the window location) increases the ACH. From the individual ACH of FDE (10.79) and FWI (33.25), the resulting ACH of the push-pull FDE-FWI (or FWI-FDE) is 46.33, which is approximately near the sum of the former individual fans. This is also true for the push-pull FDI-FWE (or FWE-FDI), where the resulting ACH is 51.6 compared to stand fan-only counterparts, FDI (39.36) and FWE (13.45). This increase in ACH is due to the flow being more directed from one side (inlet) to another side (outlet) of the room, which reduces the reversal of flow in either of the inlet and outlet boundaries, which then increases the net mass flow rate and then the ACH. *Figure 6* illustrates that for the push-full FDE-FWI, the magnitudes of the velocities at the door boundary are higher than that of a single fan FDE. Furthermore, more negative values of z-velocity in FDE of the previous study indicate more reversal of flow that was then reduced in FDE-FWI.

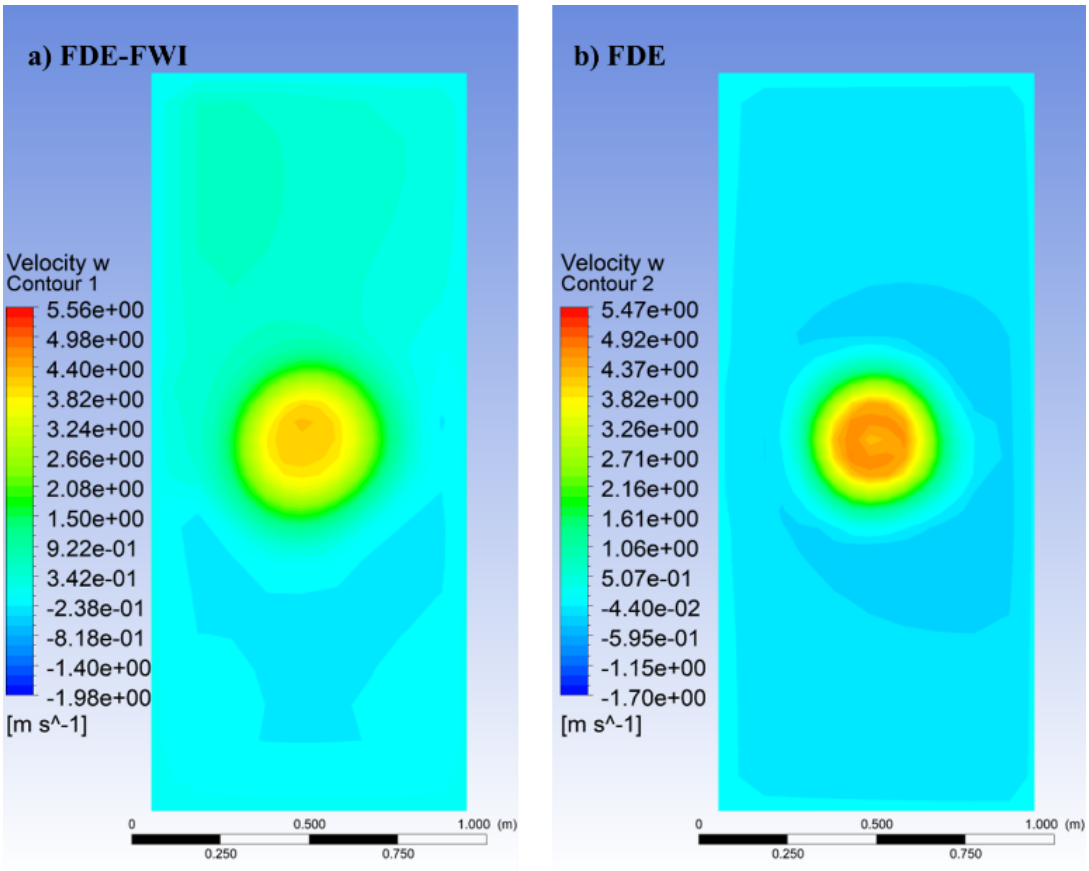

Figure 6. Comparison of Door Boundary z-velocity of a) FDE-FWI and b) FDE cases

Meanwhile, the addition of a downward ceiling fan for the intake configurations has an increase in the ACH. FDI's value has increased from 39.36 to 51.08 (FDI-CD), while FWI's value has increased from 33.25 to 55.92 (FWI-CD). This increase in ACH can be attributed to the additional suction effect made by the ceiling fan to the two intake configurations. *Figure 7*a shows the additional suction effect for FWI-CD, where the flow is directed from the window side to the inlet of the ceiling fan. This suction effect provides less reversals of flow at the window boundary that increases the velocities going inside the domain, which consequently increases the incoming volume flow rate from 0.55 m^3/s (FWI) to 0.93 m^3/s (FWI-CD), and then the ACH. On the other hand, the addition of an upward ceiling fan for the intake configurations (FDI and FWI) have resulted to different effects. FDI's value has increased by less than 1 ACH from 39.36 to 40.34 (FDI-CU), while the FWI has decreased from 33.25 to 26.35 (FWI-CU). The decrease can be attributed to the counter flow produced by the ceiling fan on the incoming flow, which is more observable in the window intake case. For example, *Figure 7*b depicts the counterflow produced in the FWI-CU case where the flow is directed from the ceiling fan outlet to the window side, thus, blocking some of the incoming flow from the window boundary and then was not able to increase the mass flow rate and the ACH. For the FDI case however, the blockage was not that comparably strong that the addition of fan did not affect the volume flow rate and the ACH.

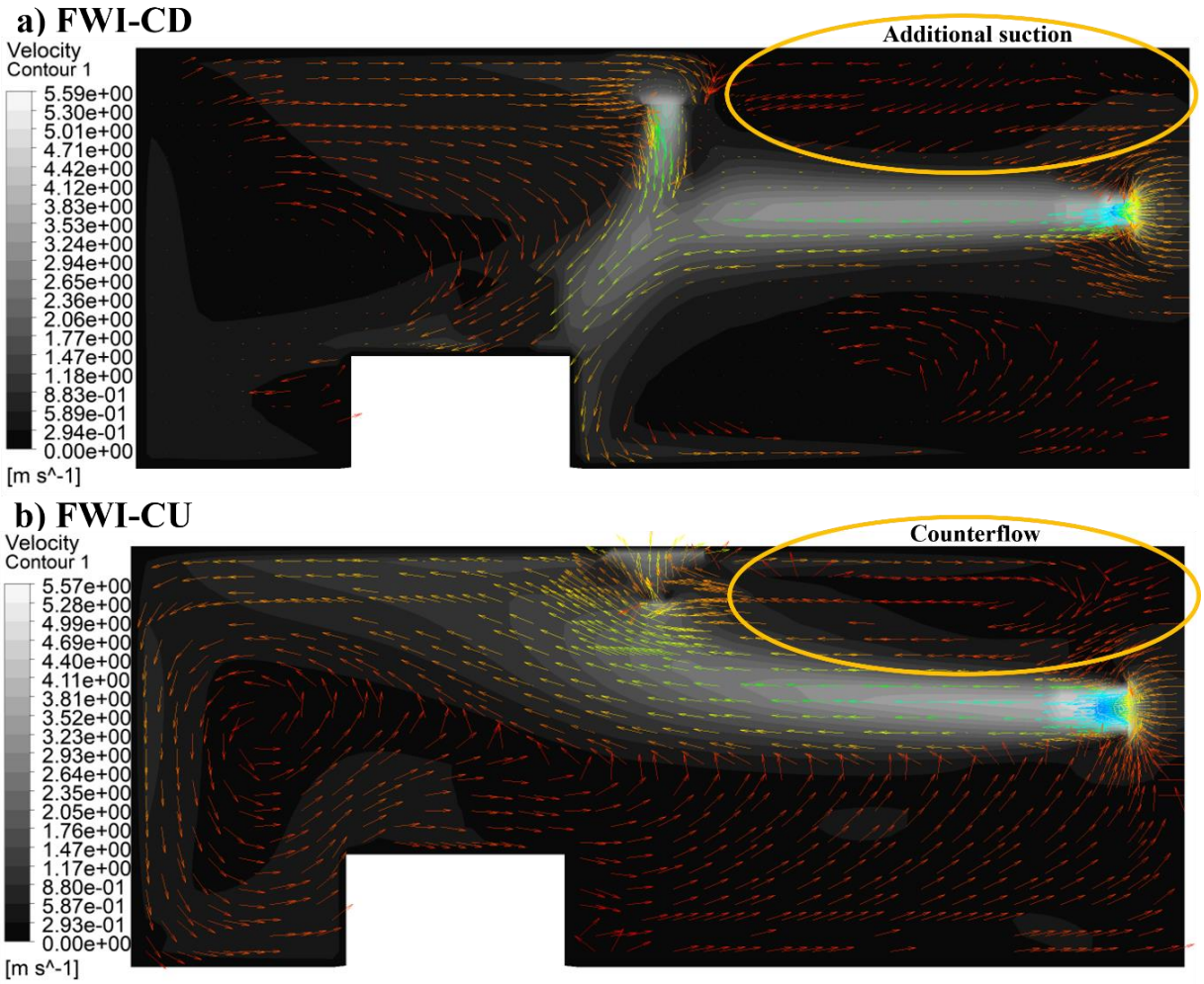

Figure 7. Velocities of Window Intake Configuration a) with Downward Ceiling Fan b) with Upward Ceiling Fan

For the exhaust cases, different behaviors can be observed between the door case and window case when ceiling fan is added. In particular, when a downward ceiling fan was added for the door exhaust case, the ACH has decreased from 10.79 to 6.88, whereas, for the window exhaust the ACH has slightly increased from 13.45 to 14.33 (*Figure 5*). On the other hand, an additional upward ceiling fan has increased the ACH of the door exhaust case from 10.79 to 19.09, while the ACH of the window exhaust has decreased from 13.45 to 3.40 (*Figure 5*). It is important to note that for exhaust cases, where the velocity fields inside the domain generally have lower values in comparison with the intake cases, the stand fans' volume of influence (where the effect of the exhaust can be felt) is low. Therefore, the behaviors in these cases are quite difficult to generalize. In addition, the actual fan distances, and the fan axis of rotation distances of the FWE-ceiling fan cases versus the FDE-ceiling fan cases are different. That can be the reason for the conflicting behaviors, which should be accounted for in future studies. Nevertheless, the FWE-CU case (*Figure 8*), with the highest decrease in ACH, has its two fans almost counteracting or pulling each other, and the window exhaust fan was forced to pull more air from the outside, therefore, doing more counterflow at the window boundary and decreases the net flow rate and then the ACH.

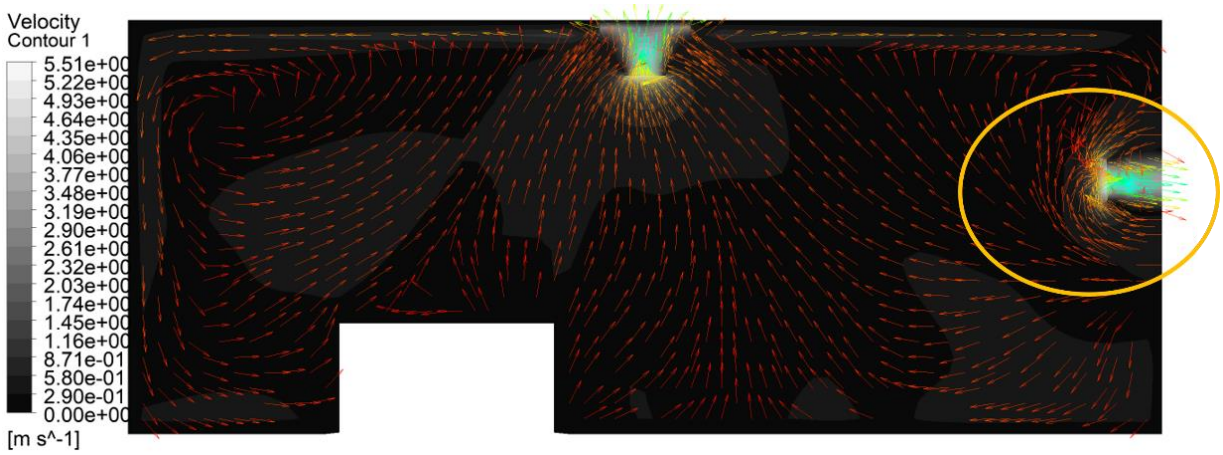

Figure 8. Velocities of Window Exhaust Configuration with Upward Ceiling Fan

The addition of fans depending on its direction, may or may help the single fan configurations in terms of ACH. Additional suction or counterflow effects at the door and window boundaries can arise, leading to the increase or decrease in the resulting boundary flow rates used to compute for the ACH. For our current set-up, the optimal combinations in terms of ACH were both the fan intake with ceiling fan facing downward configurations FDI-CD (51.08) and FWI-CD (55.92), and the two push-pull configurations FDI-FWE (51.60) and FDE-FWI (46.33), as these configurations yielded more directed flow from one boundary to another, that resulted to the increase in boundary flow rates.

3.2 Particle Dispersion

Depicted in the "stacked" bar graph (**Figure *9***) are the particle fates of the infected aerosols exhaled by the occupants M1 (**Figure *9***a) and M2 (**Figure *9***b) for all the two-fan cases together with the single-fan cases from the previous study [18]. Here, the number of particles, whether trapped on the surfaces or escaped from the boundaries, were computed, and were divided by the total number of particles exhaled by the infected occupant to get its particle percentage. In addition, we summed the particle percentage deposited on the person's body, chair, desk, and computer, as either "Trapped Source Side" or "Trapped Healthy Side". It should be noted that we only showed the bars starting from 50% as the particles that were trapped in the source side were all greater than 50%. Starting from case M1, for the push-pull configurations, FDE-FWI has only 6.38% door particle evacuation rate compared to the previous single fan configuration FDE with an evacuation rate of 27.21%. This decrease can be attributed to the higher flow rates due to higher velocities (denoted by the red streamlines in **Figure *10***) with the addition of the window intake stand fan, that might be pushing the aerosols more towards the wall where they eventually deposit (from 3.13% of FDE to 23.12% of FDE-FWI) instead of being exhausted at the door boundary. The studies of Alotaibi et al.[5], and Habchi et al. [11] showed that higher velocities drove the particles to either be confined on microclimate around the occupant or be deposited onto surfaces. It should be noted they used slightly higher particles sizes that were 1 and 0.5 microns, respectively, compared to our study which only used 0.26 microns. Nevertheless, although done in respiratory tract, Longest et al. [32] showed that inertia force can still be significant on the deposition rate of submicron particles down to 0.02 microns, which was way lower than our test case. On the other hand, FDI-FWE has an increase in window particle evacuation rate from 2.45% (FWE) to 14.96%.

The addition of FDI to FWE has increased the flow rates directed from the door to the window, thus also driving the aerosols to evacuate to the window boundary.

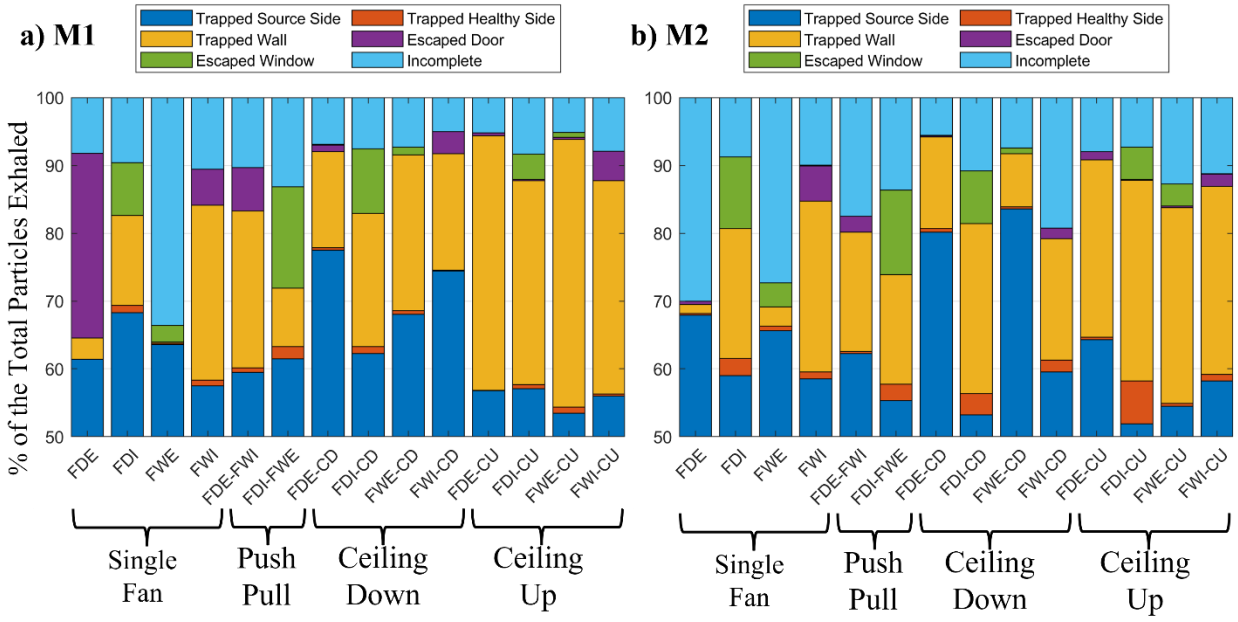

Figure 9. Particle Fate Percentage a) M1 Infected, M2 Healthy b) M2 Infected, M1 Healthy

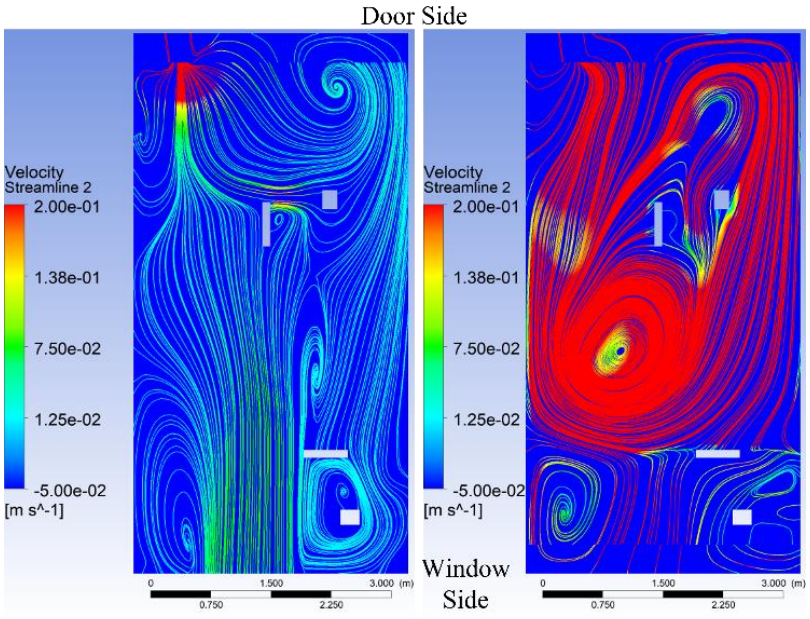

Figure 10. Velocity Profile Comparison of Cases a) FDE b) FDE-FWI

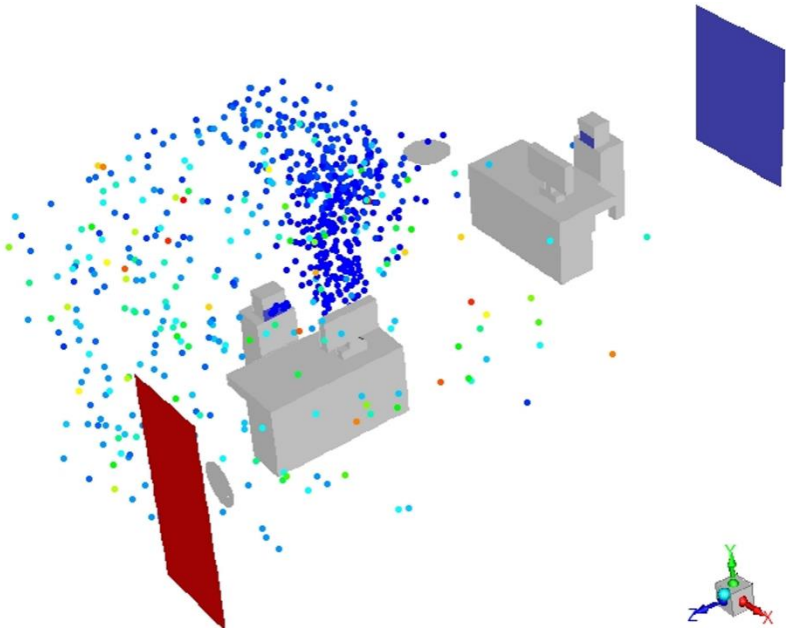

Figure 11. Particle Dispersion of FDE-CU configuration with M1 production case

For the stand fan with ceiling fan cases, regardless of ceiling fan orientation, the aerosols that are deposited to either the wall or source side have increased. This might also be due to the additional fan that increases the velocity magnitudes inside the room thus easily pushing the aerosols to the surfaces. Particularly for the cases with ceiling fans facing upwards (e.g. FDE-CU-M1 in **Figure *11***), the introduction of such fan directs the flow to the ceiling and then the particles, which then contributes to the high wall deposition (>= 30%). Moreover, there is no significant increase in the transfer of aerosols from the infected side to the healthy side.

Meanwhile, for case M2, the addition of a fan has generally no significant increase in the particle evacuation rate. Additionally, a similar trend with the M1 cases can be observed for M2 stand fan plus ceiling cases where the aerosols have an increased deposition on wall and source side surfaces. Furthermore, there is no significant difference in the transfer of aerosols from the source to the healthy side.

In addition, as our simulation has been injecting particles until the last time step, it was expected that there will still be particles inside the domain that were not yet exhausted to the boundaries or deposited on the surfaces. These were the incomplete particles. However, based on *Figure 9*, there were some cases where the percentage of the incomplete particles were relatively high, such as in the FWE of the M1 infected case, and in the FDE, FWE, FDE-FWI, and FWI-CD of the M2 infected case. This can be attributed to the particles that may have entered local vortex structures after being generated by the infected occupant. Fernandez et al. [18] already presented these near isolated vortex structures near the infected occupants for the single fan cases. This was also the reason for the two-fan configurations. As an example, *Figure 12* (FWI-CD with M2 production case) shows the local vortex structure near the infected occupant that makes the particles to circulate inside it after generation which then increases the number of incomplete

particles. The particle circulation or accumulation in the vortex structure was also evident in *Figure 15*.

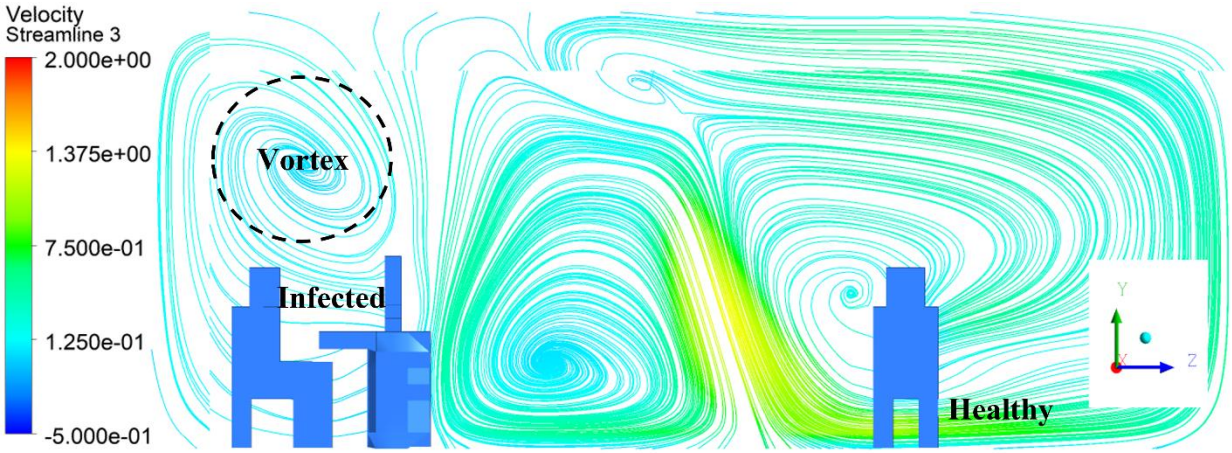

Figure 12. Local Vortex Structure Near of FWI-CD configuration with M2 production case

Overall, the effect of the additional fan in this section is the increase in velocity magnitudes and the alteration of the flow field that may or may not be beneficial to the evacuation of particles. Moreover, same with the previous study [18], even though the ACH is a measure of how well the air inside is replaced by the clean air outside, this study shows that the case with the highest ACH of 55.92 (FWI-CD) does not have a significant total evacuation rate with only 3.22% for the M1 case and 1.58% for the M2 case. In contrast, the FDE-M1 case of the previous study has a generally low ACH of 10.79 while its total evacuation rate is 27.21%. Therefore, in addition to increasing the ACH, the particle dispersion should be carefully considered to mitigate the airborne diseases transmission. Furthermore, accounting for the ACH and the particle dispersion, if the safe standard considers only the particle evacuation rate, then the FDI-FWE configuration is the best both for the M1 (51.60 ACH and 14.96% total evacuation rate) and M2 (51.60 ACH and 12.47% total evacuation rate) cases. On the other hand, if the safe standard also considers the surface deposition as it also prevents the particles to go to the healthy occupant, then the best configurations are FWI-CD (55.92 ACH and 94.82% total evacuation and deposition rate) for the M1 case and FDI-CD (51.08 ACH and 86.06% total evacuation and deposition rate) for the M2 case. It should be noted that the total evacuation rate is the sum of the percentages of the escaped window and escaped door while the total deposition rate is the sum of the trapped wall and trapped source side in *Figure 9*.

3.3 Particle Residence Time

Table 2: Maximum Particle Time in seconds of the Different Configurations and Production Cases

Source	a. Single Fan				b. Push-Pull		c. With Ceiling Downwards				d. With Ceiling Upwards			
	FDE	FDI	FWE	FWI	FDE-FWI	FDI-FWE	FDE-CD	FDI-CD	FWE-CD	FWI-CD	FDE-CU	FDI-CU	FWE-CU	FWI-CU
M1	150	175	178	175	168	174	178	153	146	157	129	146	164	129
M2	178	167	178	178	178	170	171	174	142	178	171	125	178	161

Presented in **Table *2*** are the maximum particle time (MPTs) of each of the cases. In general, the single fan cases have relatively higher MPTs with values of above 175 s except for the FDE of the M1 case of the previous study with 150 s, where the particles are exhausted in the door boundary as soon as they were generated by the infected person [18]. On the other hand, the MPTs of stand fan plus ceiling for M1 cases except for FDE-CD have decreased ranging from 129 – 164 seconds. This is primarily because of the resulting higher velocities due to an additional fan that makes the particles to be easily deposited on the surfaces after the generation event in comparison with the single fan cases. For the FDE-CD case (*Figure 13*), the addition of ceiling fan directed downwards has scattered the particles near the infected person which then produced relatively longer air suspension time.

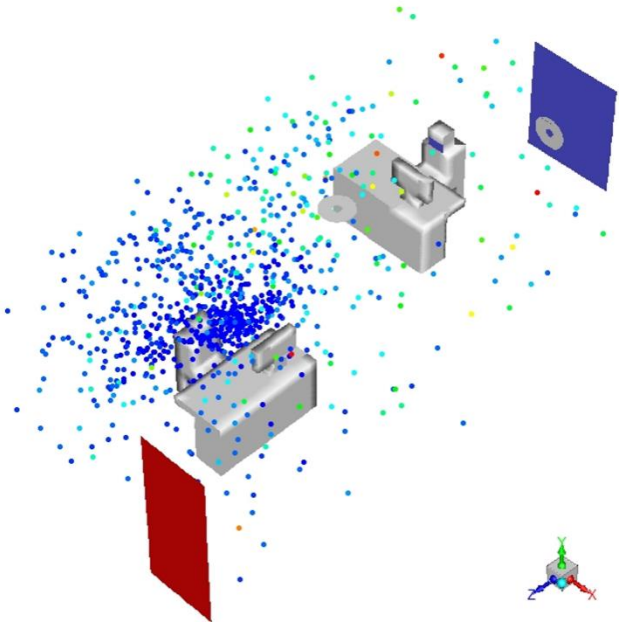

Figure 13. Particle Dispersion of FDE-CD configuration with M1 production case

In contrast, different behaviors can be observed for the M2 cases where some have retained higher MPTs. The FWE-CD and the FDI-CU cases have the lowest MPTs with values of 142 and 125, respectively. Both are primarily due to surface deposition since their respective particle evacuation (both door and window) percentages are not significantly high. On the other hand, FWE-CU (**Figure *14***) and FWI-CD (**Figure *15***), although having different configurations, have

similar circulating flow fields near the infected person that localizes the aerosols, therefore, may be the reason for higher MPTs. This flow circulation also prevented the transfer of particles from the infected to healthy occupant.

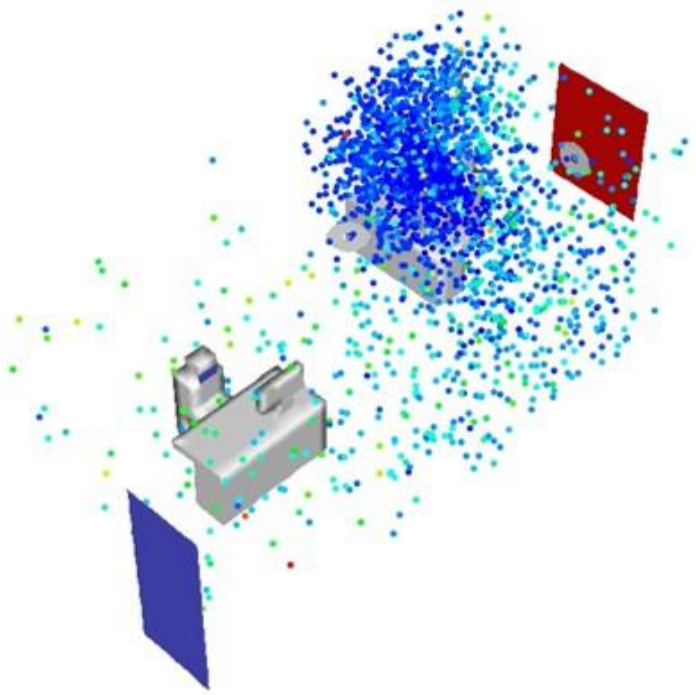

Figure 14. Particle Dispersion of FWE-CU configuration with M2 production case

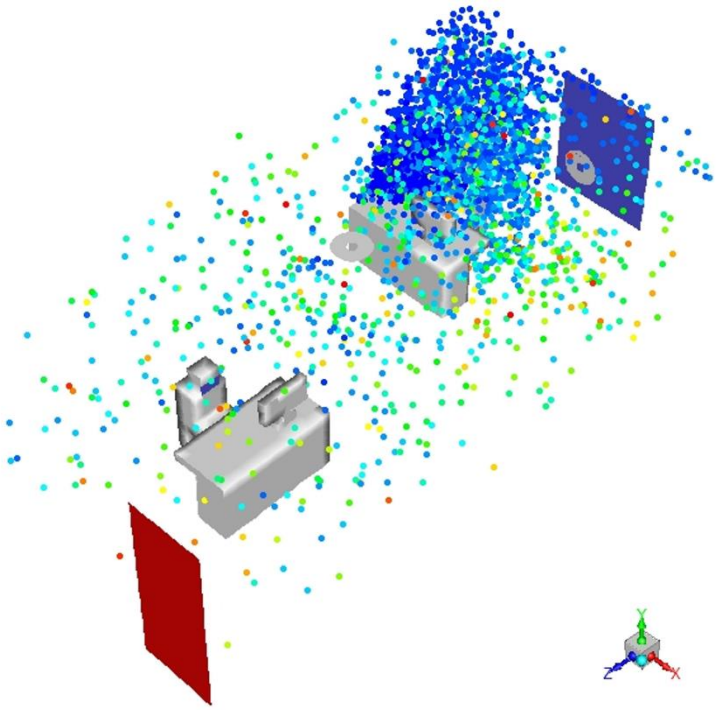

Figure 15: Particle Dispersion of FWI-CD configuration with M2 production case

In general, it was observed that there are two cases where the MPT decreases: the first one being the particles are eventually exhausted outdoors as soon as they were exhaled by the infected occupant (FDE-M1 case), and the other one being the particles are easily deposited on the surfaces due to higher velocities (most of the two-fan cases). On the other hand, MPT increases when the particles after the production event enters a region where they will circulate for longer period without deposition on surfaces or exhaustion to outdoors.

IV. CONCLUSION

In this work, 3D isothermal unsteady-RANS simulations were done to compare the effects of adding a stand fan or ceiling fan in a room with two occupants. In addition, two aerosol generation cases were conducted: one being the occupant near the door generates the particles, and the other is the occupant near the window generates the particles. The air change rate per hour (ACH), particle dispersion, and the maximum particle time were obtained for the 10 two-fan combinations and were compared with the previous single fan study.

In general, the push-pull configurations FDE-FWI and FDI-FWE, with respective ACH of 46.33 and 51.60, formed a directed flow from inlet to outlet that eliminates the reversals of flow in the boundaries, thus increasing the boundary flow rate, and then the ACH. On the other hand, the addition of ceiling fan may or may not increase the ACH depending on the resulting flow field. It will increase the ACH if the effect of ceiling fan is an induced boundary flow that has the same direction with the initially installed fan such as in the case of FWI-CD with ACH of 55.92 (highest ACH). In contrast, it will decrease the ACH if the effect of the ceiling fan is an induced boundary flow that has counter-direction with the initially installed fan such as in the case of FWE-CU with ACH of 3.40 (lowest ACH).

For the particle dispersion, the addition of fan generally increases the indoor velocity values that might be the reason that pushes the generated aerosol to deposit on the surfaces compared to the previous single fan cases as the particles followed the resulting flow field. Although, we suggest quantifying the effect of Brownian motion in future studies as the assumed particle size (0.26 microns) is within the region where the diameter is not that large for the inertia force to fully govern, and also not that large to neglect the Brownian motion. The addition of fan also altered the flow that may or may not be beneficial in contamination of cross-contamination. If the goal is to evacuate the particles outside (the safer way), the arrangement of these two-fan combinations should be carefully adjusted in such a way that the aerosols are directed to outdoors as soon as they are generated like the FDE-M1 case of the single fan configuration. Nonetheless, the easier deposition of particles due to the addition of fan prevented the aerosols from reaching the healthy occupant.

The MPT can increase or decrease depending on the particle fate. It can increase when the particles enter the recirculation or stagnation zone where they can be suspended in the air for longer period. In contrast, MPT can decrease in two ways: the first one is when the particles are eventually exhausted to outdoors as it is generated like the FDE-M1 case of the single fan configuration, the second one is when the particles are easily deposited on the surfaces due to higher velocities (most of the two-fan cases). It is also important to note that in this study having a higher ACH does not

necessarily translate to a good particle evacuation rate. For example, the FWI-CD with the highest ACH has only a 3.22% evacuation rate on the M1 production case. Therefore, even though ACH has been used as a parameter to measure ventilation, the resulting flow field and its consequent particle dispersion should have equal emphasis, as ACH is only evaluated at the boundaries (e.g. door and window) and stagnation points and recirculation zones exist inside the domain that can lead to particle accumulation and higher MPTs. Nonetheless, the previous single fan configuration FDE of the M1 case still has the highest particle evacuation rate of 27.21%, while for the two-fan configurations, the FDI-FWE of the M1 case has the highest particle evacuation rate of 14.96%.

Furthermore, the different responses of M1 and M2 cases for the same fan configurations shows that the aerosol source location has an important effect on the particle evacuation as the local flow pattern near the source will dictate the resulting dispersion. Therefore, room lay-out should also be considered to produce flow patterns that may help the exhaustion of particles to avoid cross-contamination.

It was mentioned in 3.1 that a general rule for placing two-fan combinations is difficult to establish in this study due to some conflicting trends, as the distances between the axis of rotation between the two fans are not the same. Therefore, a future study involving a more symmetrical room with same inlet and outlet boundary sizes is suggested. In addition, as we utilized the previous single fan case study settings, we were limited to the default discrete phase model software settings concerning factors such as the particle time step size. We also used a uniform particle diameter. As such, a more accurate settings for the discrete phase model can be explored in the future. Furthermore, the effect of temperature gradients may be applied as this can change the natural convection and then the growth and evaporation rates of the particles. Lastly, experimental studies through the use of fog or mist generator can also be done to mimic realistic conditions.

REFERENCES

[1] World Health Organization. Retrieved from https://www.who.int/news-room/questions-and-answers/item/coronavirus-disease-covid-19-how-is-it-transmitted on 24 July 2022.

[2] Bazant MZ, Bush JWM. 2021. A guideline to limit indoor airborne transmission of COVID-19. Proc Natl Acad Sci. USA. 118(17). doi: 10.1073/pnas.2018995118

[3] Kohanski MA, Lo LJ, Waring MS. 2020. Review of indoor aerosol generation, transport, and control in the context of COVID-19. Int Forum Allergy Rhinol. 10(10): 1173–1179. |doi: 10.1002/alr.22661

[4] Circle T, et al. 2020. ASHRAE Position Document on infectious aerosols. p. 1–24.

[5] Alotaibi S, Chakroun W, Habchi C, Ghali K, Ghaddar N. 2018. Effectiveness of contaminant confinement in office spaces equipped with ceiling personalized ventilation system. Build Simul. 11(4): 773–786. doi: 10.1007/s12273-018-0437-9

[6] Xue K, et al. 2020. Experimental study on the effect of exhaust airflows on the surgical environment in an operating room with mixing ventilation. Journal of Building Engineering. 32(April): 101837. doi: 10.1016/j.jobe.2020.101837

[7] Liu X, Lv X, Peng Z, Shi C. 2020. Experimental study of airflow and pollutant dispersion in cross-ventilated multi-room buildings: Effects of source location and ventilation path. Sustain Cities Soc. 52(September): 101822. doi: 10.1016/j.scs.2019.101822

[8] Lin T, et al. 2020. An experimental study of the flow characteristics and velocity fields in an operating room with laminar airflow ventilation. Journal of Building Engineering. 29(1): 1–9. doi: 10.1016/j.jobe.2020.101184

[9] Li W, et al. 2021. Effects of ceiling fans on airborne transmission in an air-conditioned space. Build Environ. 198(Jul). doi: 10.1016/j.buildenv.2021.107887

[10] El-Fil B, Ghaddar N, Ghali K. 2016. Optimizing performance of ceiling-mounted personalized ventilation system assisted by chair fans: Assessment of thermal comfort and indoor air quality. Sci Technol Built Environ. 22(4):412–430 doi: 10.1080/23744731.2016.1158072

[11] Habchi C, Ghali K, Ghaddar N, Chakroun W, Alotaibi S. 2016. Ceiling personalized ventilation combined with desk fans for reduced direct and indirect cross-contamination and efficient use of office space. Energy Conversion and Management. 111(March):158–173. doi: 10.1016/j.enconman.2015.12.067

[12] Gil-Baez M, Lizana J, Becerra Villanueva JA, Molina-Huelva M, Serrano-Jimenez A, Chacartegui R. 2021. Natural ventilation in classrooms for healthy schools in the COVID era in Mediterranean climate. Build Environ. 206(June): 108345. doi: 10.1016/j.buildenv.2021.108345.

[13] Hu HH. 2012. Computational fluid dynamics. Fluid Mechanics. Elsevier. p. 421–472. doi: 10.1016/B978-0-12-382100-3.10010-1

[14] Abuhegazy M, Talaat K, Anderoglu O, Poroseva SV, Talaat K. 2020. Numerical investigation of aerosol transport in a classroom with relevance to COVID-19. Physics of Fluids. 32:10. doi: 10.1063/5.0029118

[15] Lipinski T, Ahmad D, Serey N, Jouhara H 2020. Review of ventilation strategies to reduce the risk of disease transmission in high occupancy buildings. International Journal of Thermofluids. 7–8: 100045. doi: 10.1016/j.ijft.2020.100045

[16] Abdo P, Taghipour R, Huynh BP. 2020. Three-dimensional simulation of wind-driven ventilation through a windcatcher with different inlet designs. J Therm Sci Eng Appl. 12(4):1–14. doi: 10.1115/1.4045513

[17] He Y, Chu Y, Zang H, Zhao J, Song Y. 2022. Experimental and CFD study of ventilation performance enhanced by roof window and mechanical ventilation system with different design strategies. Build Environ. 224(Oct). doi: 10.1016/j.buildenv.2022.109566

[18] Fernandez KB, Dalisay JD, Berana M. 2021. Air Change and Aerosol Evacuation Rates in a Two-Occupancy Room with Stand Fan for Forced Ventilation. Philippine Engineering Journal. 42(1): 83–105.

[19] Król A, Król M. 2018. Study on numerical modeling of jet fans. Tunnelling and Underground Space Technology. 73(March):222–235. doi: 10.1016/j.tust.2017.12.024

[20] Shih TH, Liou WW, Shabbir A, Yang Z, Zhu J. 1995. A new k-ϵ eddy viscosity model for high reynolds number turbulent flows. Computer Fluids. 24(3):227-238

[21] ANSYS Fluent Users Guide.

[22] Michalcová V, Kotrasová K. 2020. The numerical diffusion effect on the cfd simulation accuracy of velocity and temperature field for the application of sustainable architecture methodology. Sustainability (Switzerland). 12(23):1–18. doi: 10.3390/su122310173

[23] Courant R, Friedrichs K, Lewy H. 1986. Über die partiellen Differenzengleichungen der mathematischen Physik. Kurt Otto Friedrichs. p. 53–95. doi: 10.1007/978-1-4612-5385-3_7
[24] Mehade Hussain S, Goel S, Kadapa C, Aristodemou E. 2022. A short review of vapour droplet dispersion models used in CFD to study the airborne spread of COVID19. Mater Today Proc. 64: 1349–1356. doi: 10.1016/j.matpr.2022.03.724
[25] Zhuang X, Xu Y, Zhang L, Li X, Lu J. 2022. Experiment and numerical investigation of inhalable particles and indoor environment with ventilation system. Energy Build. 271(Sept). doi: 10.1016/j.enbuild.2022.112309
[26] Liu S, Koupriyanov M, Paskaruk D, Fediuk G, Chen Q. 2022. Investigation of airborne particle exposure in an office with mixing and displacement ventilation. Sustain Cities Soc. 79(Apr). doi: 10.1016/j.scs.2022.103718
[27] Li H, Zhong K, Zhai Z(J). 2020. Investigating the influences of ventilation on the fate of particles generated by patient and medical staff in operating room. Build Environ. 180(Apr): 1–11. doi: 10.1016/j.buildenv.2020.107038
[28] Kumar S, King MD. 2022. Numerical investigation on indoor environment decontamination after sneezing. Environ Res. 213(Oct) doi: 10.1016/j.envres.2022.113665
[29] Pourdeyhimi B. 2020. Surgical mask particle filtration efficiency (PFE). The Journal of Science and Medicine. 2(3):1–11. doi: 10.37714/josam.v2i4.50
[30] Milton DK, Fabian MP, Cowling BJ, Grantham ML, McDevitt JJ. 2013. Influenza virus aerosols in human exhaled breath: Particle size, culturability, and effect of surgical masks. PLoS Pathog. 9(3). doi: 10.1371/journal.ppat.1003205
[31] Nicas M, Nazaroff WW, Hubbard A. 2005. Toward understanding the risk of secondary airborne infection: Emission of respirable pathogens. Journal of Occupational and Environmental Hygiene 2(3):143–154. doi: 10.1080/15459620590918466
[32] Longest PW, Xi J. 2007. Computational investigation of particle inertia effects on submicron aerosol deposition in the respiratory tract. Journal of Aerosol Science. 38(1):111–130 doi: 10.1016/j.jaerosci.2006.09.007